PAPER

A new algorithm for frequency-dependent shear-wave splitting parameters extraction

J. Geophys. Eng. **10** (2013) 055005 (7pp) doi:10.1088/1742-2132/10/5/055005

A new algorithm for frequency-dependent shear-wave splitting parameters extraction

Jian-li Zhang[1,2], **Yun Wang**[3] **and Jun Lu**[4]

[1] Multi-Wave and Multi-Component (MWMC) Group, Institute of Geology and Geophysics, Chinese Academy of Sciences, Beijing 100029, People's Republic of China
[2] University of Chinese Academy of Sciences, Beijing 100049, People's Republic of China
[3] Multi-Wave and Multi-Component (MWMC) Group, Institute of Geochemistry, Chinese Academy of Science, Guiyang 550002, People's Republic of China
[4] The Key Laboratory of Marine Reservoir Evolution and Hydrocarbon Accumulation Mechanism, Ministry of Education of China, China University of Geosciences, Beijing 100083, People's Republic of China

E-mail: yunwang@mail.iggcas.ac.cn

Received 16 November 2012
Accepted for publication 2 May 2013
Published 20 September 2013
Online at stacks.iop.org/JGE/10/055005

Abstract
In the exploration of a fractured reservoir, it is very important for reservoir engineers to get information about fracture sizes, because macro-scale fractures are more significant to the control of reservoir storability and fluid flow even though both micro-scale cracks and macro-scale fractures contribute to the dominant anisotropy. Recently, a poroelastic equivalent medium model was proposed by Chapman, which describes the frequency-dependent anisotropy effect with the fracture size being one of the key parameters. Based on this model, geophysicists have done work to measure fracture sizes from seismic data. However, it is necessary to extract frequency-dependent anisotropy before inverting for fracture size. In this paper, a new algorithm is developed for extracting frequency-dependent anisotropic parameters from surface multi-component seismic data, especially from a common-receiver-gather. Compared with the conventional method of extracting the splitting parameters only for different frequency bands, it is possible to extract splitting parameters for each frequency with the new algorithm. To check the reliability of the algorithm, a common-receiver-all-azimuth-gather is synthesized by the vector convolution method, involving the splitting parameters dependent on frequency. Test results show that the frequency-dependent splitting parameters will be extracted accurately with a general level of noise (the signal to noise ratio, SNR for shot, equals 3). More importantly, under the joint constraints of multi-azimuth data, a satisfactory result will be obtained even if the noise is significant (SNR equals 1). The good performance of the algorithm in a model test indicates its potential for field applications.

Keywords: fracture detection, frequency-dependent, frequency-domain, layer stripping

1. Introduction

The presence of fractures in hydrocarbon reservoirs can enhance porosity and permeability, and can consequently increase production. Thus, the characteristic parameters of fracture systems, including fracture orientation, density and fracture size, are necessary information for reservoir engineers. One of the most successful methods for the detection and characterization of fractures is the use of shear-wave splitting (Crampin 1981, 1984). Through the analysis of shear-wave splitting, fracture orientation can be inferred from the polarization direction of a fast S-wave, whereas fracture

density can be estimated from the time-delay between fast and slow S-waves. Therefore, the use of shear-wave splitting to characterize fracture systems has been paid plenty of attention in the last two decades (Silver and Chan 1991, Li and MacBeth 1997, Wang *et al* 2003, Wei 2004, Crampin and Gao 2006, Tian *et al* 2011). Dozens of methods have been developed to extract the splitting parameters from both the surface multi-component seismic data (Dumitru and Bale 2000, Gao *et al* 2006, Zhang *et al* 2012) and VSP logging data (Alford 1986, Lefeuvre *et al* 1992, Li and Crampin 1993, Zeng and Macbeth 1993). However, it is still not possible to estimate fracture sizes, which are very important to reservoir engineers, with these conventional methods. It is thought that although both micro-scale cracks and macro-scale fractures can contribute to the dominant anisotropy, the latter is much more important as it controls reservoir storability and fluid flow (Maultzsch *et al* 2003). Recent research has shown that frequency-dependent shear-wave splitting is very sensitive to fracture size (Liu *et al* 2003). Low frequencies would reflect information about macro-scale fractures while high frequencies are more sensitive to micro-scale cracks (Liu *et al* 2006). However, it is difficult to explain the frequency-dependent anisotropy (FDA) effect using traditional equivalent medium theories (e.g. Hudson 1981, Thomsen 1995) which predict frequency-independent behaviour. Recently, a poroelastic equivalent medium model was proposed by Chapman (2003) to address this question; it describes the FDA effect with the size of the fractures being one of the key parameters. Based on this model, it becomes possible to measure the fracture size from seismic data.

In the past ten years, the FDA effect has been observed in earthquake data (Marson-Pidgeon and Savage 1997, Liu *et al* 2001, Gao *et al* 2010), multi-component VSP data (Chesnokov *et al* 2001, Liu *et al* 2003), and also microseismic data (Al-Anboori *et al* 2006). Based on Chapman's model, Maultzsch *et al* (2003) modelled frequency-dependent shear-wave splitting in multi-component VSP data from a tight gas reservoir and successfully obtained the size of fractures. Al-Harrasi *et al* (2011) carried out similar work on microseismic data and also got a relatively satisfactory result. According to the equivalent medium theory by Chapman, it is necessary to extract FDA first before inverting for fracture density and fracture size. For the conventional extraction method, a conventional shear-wave splitting algorithm is applied to different band-pass datasets to obtain the splitting parameters for different frequency bands (Maultzsch *et al* 2003); nevertheless, it is impossible to extract splitting parameters for each frequency with this conventional method. In order to obtain the splitting parameters for each frequency, Han and Zeng (2011) developed an algebraic technique to extract splitting parameters from VSP multi-component data. However, this algorithm was mainly for four-component VSP logging data, whereas most field shear-wave recordings are obtained from surface seismic data. Besides, compared to the VSP data with large space limitations, the surface seismic data is characterized by good spatial continuity. Therefore, it is necessary to develop a method to extract frequency-dependent anisotropic parameters from surface multi-component seismic data.

In this paper, based on the vector convolution model proposed by Zeng and Macbeth (1998), we propose a new algorithm for extracting frequency-dependent splitting parameters from surface data, especially from a common-receiver-gather dataset. And following the description of the algorithm, a common-receiver-all-azimuth-gather dataset is synthesized to test the reliability of the algorithm.

2. Method and principle

In order to clarify the description, we assume that the response of the earth is linear, and the shear wave takes a linear polarization in a particular direction. Only the vertical incidence case is considered in this section, but it is deemed to work well in near-offset. On the ground a geophone with two horizontal components is used to record the seismic waveform, of which one component is aligned along the radial direction (R) and the other along the transverse direction (T). The source will excite waves polarized along the orthogonal fast and slow directions (f- and s-axes). The polarization direction of an initial converted shear wave is assumed to be along the radial direction for further simplicity.

Based on the above assumptions, the projection vector $\mathbf{S}_p(t)$ of an initial converted shear wave $\mathbf{S}(t)$ in the $f-s$ natural coordinate frame can be written as

$$\mathbf{S}_p(t) = \begin{bmatrix} S_f(t) \\ S_s(t) \end{bmatrix} = \begin{bmatrix} \cos\varphi \\ -\sin\varphi \end{bmatrix} S(t), \tag{1}$$

where the subscripts f and s refer to fast and slow directions, respectively; φ denotes the fracture azimuth.

Based on the vector convolution model of Zeng and Macbeth (1998), the propagation vector $\mathbf{d}_p(t)$ composed of fast and slow components will be generated when the initial linearly polarized shear wave propagates into the extensive-dilatancy anisotropic media. The above process can be expressed as

$$\mathbf{d}_p(t) = \begin{bmatrix} d_f(t) \\ d_s(t) \end{bmatrix} = \mathbf{\Lambda}(t) * \mathbf{S}_p(t), \tag{2}$$

where $d_f(t)$ and $d_s(t)$ denote fast and slow components excited respectively. The star symbol ($*$) denotes a convolution in the time domain. The operator $\mathbf{\Lambda}(t)$ is given by

$$\mathbf{\Lambda}(t) = \begin{bmatrix} \lambda_f(t) & 0 \\ 0 & \lambda_s(t) \end{bmatrix}. \tag{3}$$

In the time domain, $\lambda_f(t)$ and $\lambda_s(t)$ convolve with the source wavelet $S(t)$ to produce the amplitude and time-delay of fast and slow components:

$$\begin{aligned} \lambda_f(t) * S(t) &= a_f * S(t - t_f) \\ \lambda_s(t) * S(t) &= a_s * S(t - t_s), \end{aligned} \tag{4}$$

where t_f and t_s are the travel times of fast and slow arrivals, respectively.

Just as figure 1 showed, after a rotation transformation for propagation vector $\mathbf{d}_p(t)$ from a natural coordinate frame to an acquisition coordinate frame, the acquisition vector $\mathbf{d}(t)$, composed of radial and transverse components, can be written as

$$\mathbf{d}(t) = \begin{bmatrix} d_R(t) \\ d_T(t) \end{bmatrix} = \mathbf{R}^T(\varphi)\mathbf{d}_p(t) = \mathbf{R}^T(\varphi)\mathbf{\Lambda}(t) * \mathbf{S}_p(t), \tag{5}$$

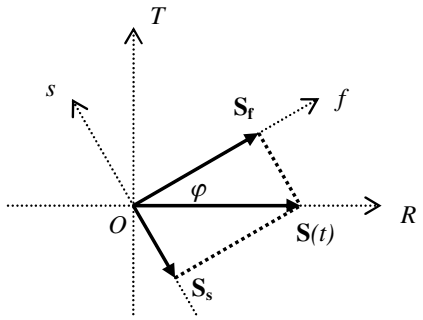

Figure 1. Coordinate system in the horizontal plane, where $f-s$ denotes the natural coordinate frame, and $R-T$ represents the acquisition coordinate frame; φ denotes the fracture orientation.

where $d_R(t)$ and $d_T(t)$ represent the observed radial and transverse components respectively. $\mathbf{R}(\varphi)$ is the rotation matrix, given by

$$\mathbf{R}(\varphi) = \begin{bmatrix} \cos\varphi & \sin\varphi \\ -\sin\varphi & \cos\varphi \end{bmatrix}. \tag{6}$$

Multiplied by the orthogonal matrix $\mathbf{R}(\varphi)$ on the left-hand side, equation (6) can be written as

$$\mathbf{R}(\varphi)\mathbf{d}(t) = \mathbf{\Lambda}(t) * \mathbf{S}_p(t). \tag{7}$$

Equation (7) can be expanded as

$$\begin{bmatrix} d_R(t)\cos\varphi + d_T(t)\sin\varphi \\ -d_R(t)\sin\varphi + d_T(t)\cos\varphi \end{bmatrix} = \begin{bmatrix} \cos\varphi \cdot \lambda_f(t) * S(t) \\ -\sin\varphi \cdot \lambda_s(t) * S(t) \end{bmatrix}. \tag{8}$$

Note that in the frequency domain, $\lambda_{f,s} = A_{f,s}\exp(-\mathrm{i}\omega t_{f,s})$. Taking the Fourier transform on both sides of equation (8), we can get

$$\begin{bmatrix} d_R(\omega)\cos\varphi + d_T(\omega)\sin\varphi \\ -d_R(\omega)\sin\varphi + d_T(\omega)\cos\varphi \end{bmatrix} = \begin{bmatrix} A_f\exp(-\mathrm{i}\omega t_f)S(\omega)\cos\varphi \\ -A_s\exp(-\mathrm{i}\omega t_s)S(\omega)\sin\varphi \end{bmatrix}. \tag{9}$$

After dividing the upper equation by the lower, we have

$$\frac{d_R(\omega)\cos\varphi + d_T(\omega)\sin\varphi}{-d_R(\omega)\sin\varphi + d_T(\omega)\cos\varphi} = \frac{\cos\varphi}{-\sin\varphi}\frac{A_f}{A_s}\exp[\mathrm{i}\omega(t_s - t_f)]\frac{S(\omega)}{S(\omega)}. \tag{10}$$

Assuming that the amplitude attenuation of the fast and slow wave is equal, that is $A_f/A_s = 1$, after a modulus calculation of equation (10), the following equation can be derived

$$P(\omega)\sin 2\varphi - Q(\omega)\cos 2\varphi = 0. \tag{11}$$

Meanwhile,

$$\begin{cases} P(w) = \mathrm{RE}_R(\omega)\mathrm{RE}_T(\omega) + \mathrm{IM}_R(\omega)\mathrm{IM}_T(\omega) \\ Q(w) = \mathrm{AM}_T^2(\omega), \end{cases}$$

where RE and IM denote the real and imaginary parts of the imaginary numbers, respectively, and AM stands for the amplitude.

Equation (11) is set up for any frequency, obviously; nevertheless, equation (11) is difficult to satisfy for the field data due to factors such as noise, non-vertical incidence and geophone mis-coupling. Therefore, we solve the above equation for real data by minimizing the target energy function $E(\varphi)$:

$$E(\varphi) = (P\sin 2\varphi - Q\cos 2\varphi)^2. \tag{12}$$

Satisfactory points will be obtained by calculating $E'(\varphi) = 0$, where the prime ($'$) refers to differentiation. It gives

$$\varphi_k = \frac{1}{2}\arctan(Q/P) + \frac{k\pi}{2}, \tag{13}$$

where k is any integer. There are two solutions for φ in the range of $0 \sim \pi$, which are separated by $\pi/2$, of which one corresponds to the minimum value of $E(\varphi)$ and the other to the maximum. The true value will be fixed by calculating the second differentiation of $E(\varphi)$. Taking the acquired fast azimuth φ back to equation (10), we can obtain the time-delay of the fast and slow shear waves from the expression

$$\delta t = t_s - t_f = -\frac{1}{2\pi f}\arccos\frac{-\tan\varphi(P\cos 2\varphi + W\sin 2\varphi)}{W\cos 2\varphi - P\sin 2\varphi + \left(AM_R^2 + AM_T^2\right)/2} + \frac{k}{f}, \tag{14}$$

where $W(\omega) = \frac{1}{2}\left(AM_T^2(\omega) - AM_R^2(\omega)\right)$.

In the converted wave field exploration, one type of geometry arrangement, involving one common geophone and multi-azimuth shots, is usually adopted to improve the inversion precision of fracture parameters. Therefore, it is meaningful to develop an FDA extracting algorithm, particularly for a common-receiver-multi-azimuth-gather dataset. Following the above derivation process, in the case of a common-receiver-multi-azimuth-gather, a similar target energy function, $E(\varphi)$, will be obtained for N shots:

$$E(\varphi) = \sum_{j=1}^{N}(P_j\sin 2(\varphi + \xi_j) - Q_j\cos 2(\varphi + \xi_j))^2, \tag{15}$$

where ξ denotes the angle between the azimuth of the target trace and the other used trace in the horizontal plane; $\xi_1 = 0$ here. P_j and Q_j can be calculated with seismic data of the jth trace. By calculating the equation of $E'(\varphi) = 0$, the solution expression of the fast azimuth will be obtained for each frequency:

$$\varphi_k = \frac{1}{4}\arctan\left(\frac{2\sum P_jQ_j\cos 4\xi_j - \sum\left(P_j^2 - Q_j^2\right)\sin 4\xi_j}{2\sum P_jQ_j\sin 4\xi_j + \sum\left(P_j^2 - Q_j^2\right)\cos 4\xi_j}\right) + \frac{k\pi}{4}, \tag{16}$$

where k can take any integer value. There are four solutions for φ in the range of $0 \sim \pi$, which are separated by $\pi/4$, of which a couple separated by $\pi/2$ correspond to the minimum value of $E(\varphi)$ representing the fast and slow polarization, respectively. Further, the correct solution will be obtained by calculating the second differentiation of $E(\varphi)$.

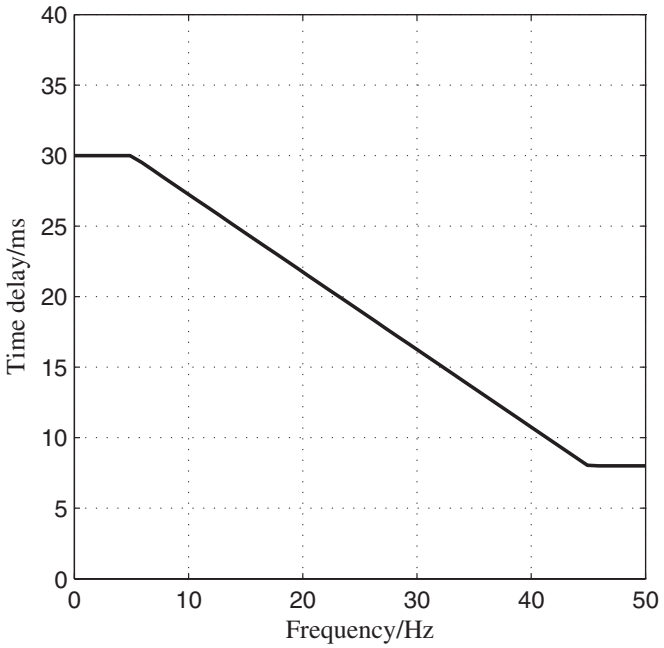

Figure 2. The frequency-dependent time delay designed for the model test.

3. Synthetic data test

A common-receiver-all-azimuth-gather dataset is synthesized to test the performance and reliability of our algorithm. We construct a simple anisotropic one-layer model involving FDA. The frequency-dependent time-delay designed beforehand is shown in figure 2. It is set that the time-delay takes a linear decrease with a frequency in the range of 5–45 Hz, while the fast polarization is independent of frequency. We synthesize two-horizontal-component recordings of 36 shots at near-offset. These shots are assumed to be equally spaced in the 10°–360° azimuth zone at 10° intervals, and the azimuth of the first shot is set parallel with the fast polarization. The synthetic seismograms for all-azimuth radial and transverse components are calculated for 1 s length at a 1 ms sample interval with the vector convolution method, as shown in figure 3. The source peak frequency is 25 Hz.

Figure 3 has presented strong azimuth anisotropy in radial and transverse components due to shear-wave splitting. Firstly, the fast orientation should be obtained before extracting the frequency-dependent time-delay. Under noise-free conditions, the new algorithm was applied for the synthetic data to extract frequency-dependent fast orientations for each trace with only the single azimuth data constrained. Figure 4 shows the inversion results in the frequency range of 5–45 Hz for the 5°–85° azimuth zone. It is apparent that the fast orientation is accurately extracted for each trace and each frequency, demonstrating the validity of the algorithm.

Because the multi-component surface data is usually characterized by a low SNR, it is necessary to test the robustness of the new method under noisy conditions. Figure 5 displays the inversion results under noisy conditions (the SNR equals 3) for the same frequency and azimuth zone as in figure 4. The errors of fast orientation begin to appear in all of the range, especially in the low-frequency domain where errors are too large to be ignored (figure 5). However, what should be noted is that the inversion result is satisfactory as a whole, even under a strong noise background with SNR equal to 3. It is certain that the inversion precision that is only single-azimuth constrained will be lower than that which is multi-azimuth

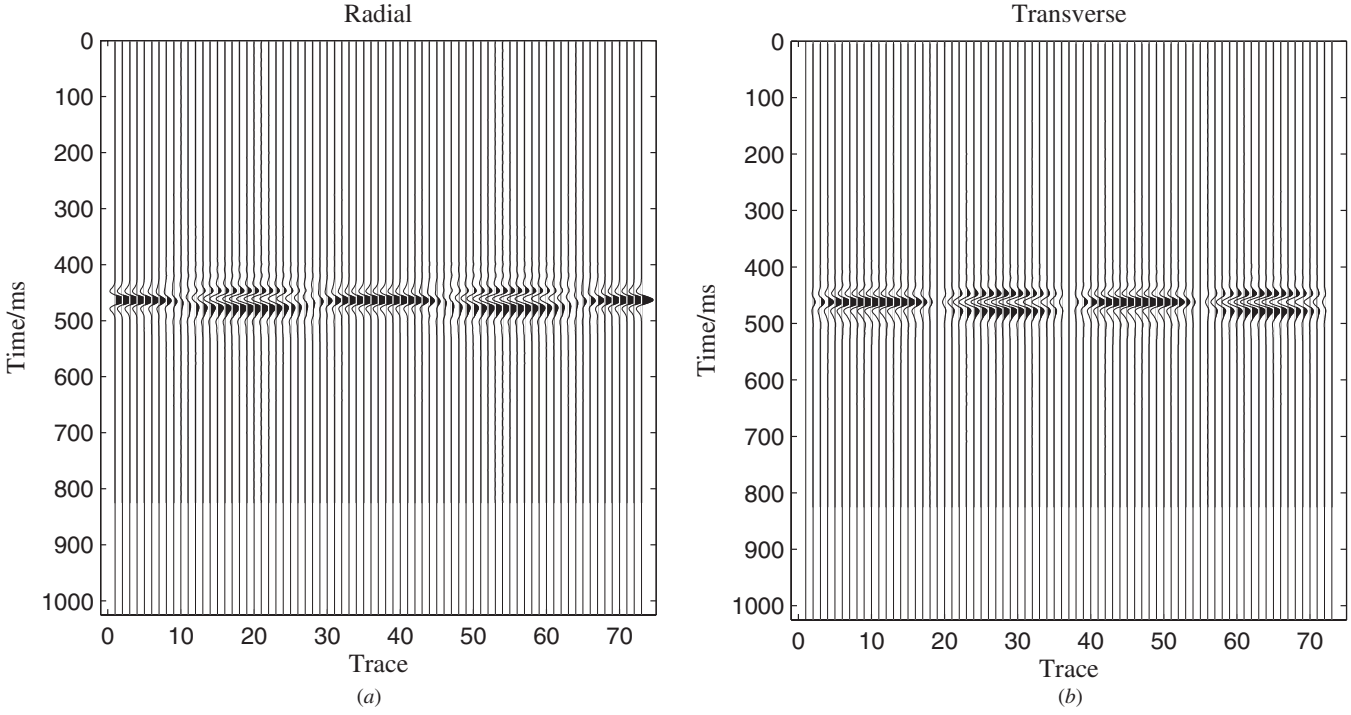

Figure 3. The radial (*a*) and transverse (*b*) components of a common-receiver-all-azimuth-gather synthesized by the vector convolution method.

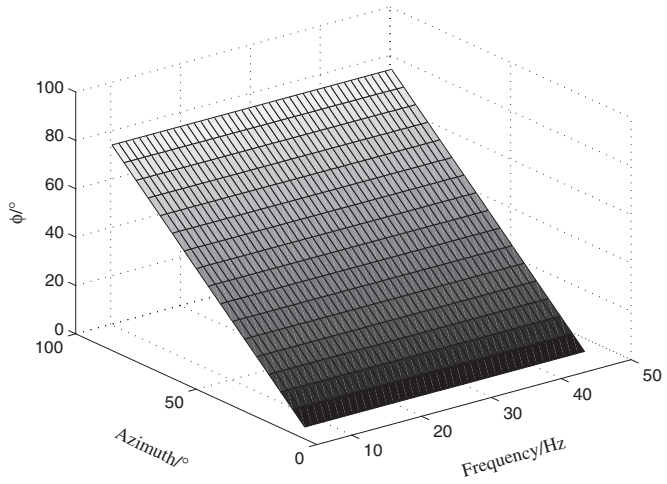

Figure 4. The frequency-dependent fast orientations extracted for the synthetic dataset with only the single-azimuth data constrained under noise-free conditions.

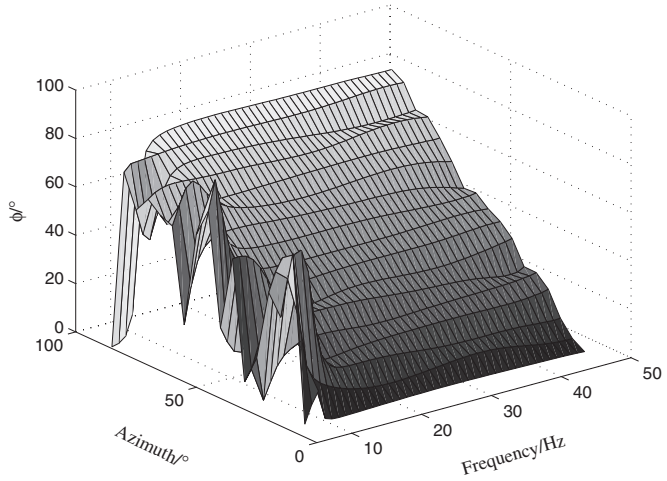

Figure 5. The frequency-dependent fast orientations extracted with only single-azimuth data constrained, when the SNR equals 3.

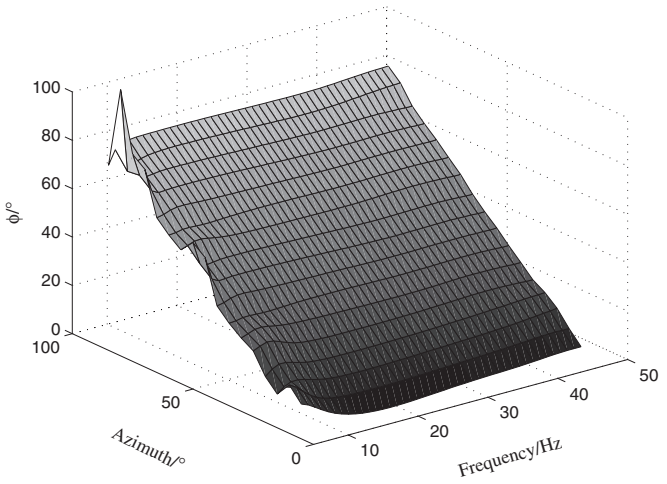

Figure 6. The frequency-dependent fast orientations extracted for the same noisy data as in figure 5, by the multi-azimuth constraint technique.

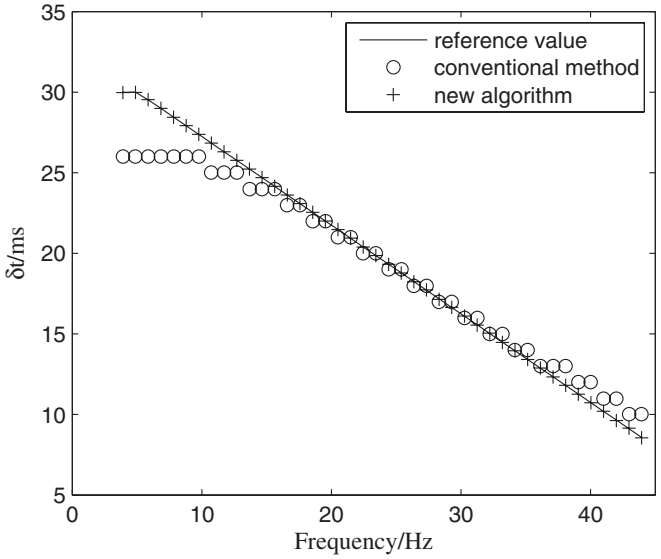

Figure 7. The frequency-dependent time delay extracted with the new algorithm and the conventional method, respectively, under noise-free conditions.

constrained. To test the performance of the multi-azimuth constrained technique, we applied this technique to the same noisy dataset with a constraint azimuth interval of 25° on the basis of equation (16), which means extracting the splitting parameters of one target trace with the joint constraint of six traces. The inversion results (figure 6) are extremely close to the theoretical value in figure 4, except for some values at the low-frequency interval. The strong contrast between figures 5 and 6 demonstrates that the multi-azimuth constraint technique is more precise than the single-azimuth constraint technique. In order to quantify the robustness of these two techniques, we perform a statistical analysis on the extracted fast orientations at a fixed frequency but at different noise levels. 200 tests are carried out under two different noisy conditions (SNR = 1 and SNR = 3, respectively) with a frequency of 30 Hz and a 30° azimuth. The statistical analysis of these tests show that the errors of the single-azimuth-constraint technique and the multi-azimuth technique are about 4° and ∼2°, respectively, when the SNR is set to 3, while they are 8° and 3.5° when the SNR equals 1. These results further confirm the reliability of the new algorithm, especially the strong robustness of the multi-azimuth constraint technique.

The frequency-dependent time-delay can be extracted using equation (14) following the acquisition of the fast orientation. Figure 7 shows the comparison of the new algorithm with the conventional narrow-band filter method in the frequency range of 5–45 Hz under noise-free conditions. The conventional method applies Alford rotation to 8 Hz-width band-pass datasets (Maultzsch *et al* 2003) and regards the central frequency of the frequency band as the target frequency. Figure 7 shows that the frequency-dependent time delays extracted with the new algorithm are coincident with the reference values, while those extracted by the conventional method exhibit an error larger than 3 ms at some frequency intervals, which indicates the superiority of the new algorithm over the conventional method.

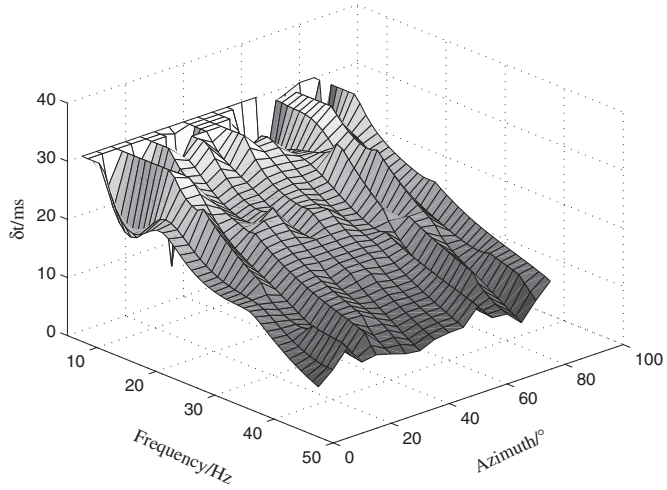

Figure 8. The frequency-dependent time delays extracted for the same noisy data as in figure 5 by the single-azimuth constrained technique.

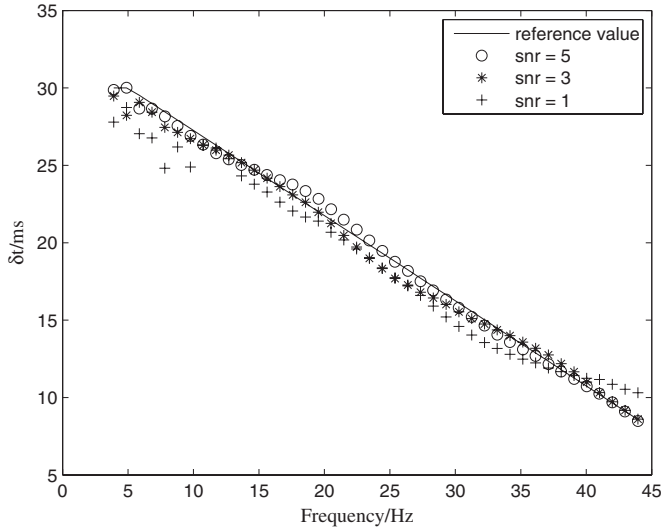

Figure 9. A statistical analysis of extracted time delays by the averaging technique in a 5°–85° azimuth zone when the SNR equals 5 (denoted by an empty circle), 3 (denoted by a star) and 1 (denoted by a cross), respectively.

Considering the low SNR of surface data, it is necessary to test the performance of the new algorithm in noisy conditions. Figure 8 shows the extracted time delays in the frequency range of 5–45 Hz for a 5°–85° azimuth zone under noisy conditions (SNR equals 3). Figure 8 shows that the FDA is correctly extracted on the whole, although the errors of time delay in some intervals are too large to be ignored. Because the recordings of a common-receiver-near-offset-gather mainly reflect the same underground structure, it is feasible and useful to average the time delay for each frequency in a certain azimuth region. Figure 9 shows the result of statistical analysis on the extracted time delay with the averaging technique in a 5°–85° azimuth zone under different noisy conditions (SNR equals 5, 3 and 1, respectively). It can be concluded that the error of time delay is less than 3 ms even when the SNR equals 1, and for the general level of noise the error cannot exceed 2 ms (figure 9), which demonstrates the strong robustness of the averaging technique.

Overall, it should be noted that the multi-azimuth constraint technique is confirmed to be of strong robustness, and the averaging technique for extracting the time-delay can also be regarded as one kind of multi-azimuth constraint technique. Therefore, it will be very helpful for fracture detection to acquire seismic data from different azimuths as much as possible in field exploration.

4. Conclusion

Based on a poroelastic equivalent medium model proposed by Chapman, measuring fracture sizes from seismic data becomes possible. However, the frequency-dependent anisotropy must be extracted before inverting for fracture size. In this paper, a new algorithm is developed for extracting frequency-dependent splitting parameters from surface multi-component data, especially from a common-receiver-gather. Compared with the conventional method, it is possible to extract splitting parameters for each frequency with the new algorithm rather than only extracting the splitting parameters for different frequency bands. A common-receiver-all-azimuth-gather is synthesized to check the reliability of the algorithm. Test results show that the frequency-dependent splitting parameters will be extracted accurately with the new algorithm under noisy conditions. In particular, a result of high precision will be obtained when using the multi-azimuth constraint technique. A statistical analysis on noise tests shows that the error of fast orientation extracted with multi-azimuth constraint technique is less than 4°, and that of the time-delay technique is less than 3 ms, with the SNR assumed as 1. The strong robustness of the new algorithm, especially the multi-azimuth constraint technique, indicates its potentiality in field application.

Acknowledgements

The research is supported by the China National Special Fund (nos 2011ZX05035-001-006HZ, 002-003HZ and 008-006-022), the PetroChina Innovation Foundation (2011D-5006-0303) and the NSFC (4110484). We thank Dr Zhaoxia Jiang for her help in preparing our paper.

References

Al-Anboori A, Kendall J and Chapman M 2006 Fracture-induced frequency-dependent anisotropy, Yibal Field, Oman *Proc. EAGE 68th Conf. and Technical Exhibition (Vienna, Austria)* p A047 (Expanded Abstracts)

Alford R M 1986 Shear data in the presence of azimuthal anisotropy *Society of Exploration Geophysicists Annu. Meeting (Dilly, TX, 2–6 Nov.)* pp 476–9 (Expanded Abstracts)

Al-Harrasi O H, Kendall J M and Chapman M 2011 Fracture characterization using frequency-dependent shear wave anisotropy analysis of microseismic data *Geophys. J. Int.* **185** 1059–70

Chapman M 2003 Frequency-dependent anisotropy due to meso-scale fractures in the presence of equant porosity *Geophys. Prospect.* **51** 369–79

Chesnokov E *et al* 2001 Frequency dependent anisotropy *Society of Exploration Geophysicists Annu. Meeting (San Antonio, TX, Sept. 9–14)* vol 20 pp 2120–3 (Expanded Abstracts)

Crampin S 1981 A review of wave motion in anisotropic and cracked elastic-media *Wave Motion* **3** 343–91
Crampin S 1984 An introduction to wave propagation in anisotropic media *Geophys. J. Int.* **76** 17–28
Crampin S and Gao Y 2006 A review of techniques for measuring shear-wave splitting above small earthquakes *Phys. Earth Planet. Inter.* **159** 1–14
Dumitru G and Bale R 2000 Minimum entropy rotation: a new shear-wave splitting technique for converted wave data *Society of Exploration Geophysicists Annu. Meeting (Calgary, Alberta, Aug. 6–11)* pp 1229–32 (Expanded Abstracts)
Gao Y, Hao P and Crampin S 2006 SWAS: a shear-wave analysis system for semi-automatic measurement of shear-wave splitting above small earthquakes *Phys. Earth Planet. Inter.* **159** 71–89
Gao Y, Wu J, Yi G X and Shi Y T 2010 Crust-mantle coupling in North China: preliminary analysis from seismic anisotropy *Chin. Sci. Bull.* **55** 2837–43
Han K and Zeng X 2011 Algebraic processing technique for extracting frequency-dependent shear-wave splitting parameters in an anisotropic medium *Appl. Geophys.* **8** 134–40
Hudson J A 1981 Wave speeds and attenuation of elastic waves in material containing cracks *Geophys. J. R. Astron. Soc.* **64** 133–50
Lefeuvre F, Nicoletis L, Ansel V and Cliet C 1992 Detection and measure of the shear-wave birefringence from vertical seismic data: theory and applications *Geophysics* **57** 1463–81
Li X-Y and Crampin S 1993 Linear-transform techniques for processing shear-wave anisotropy in four-component seismic data *Geophysics* **58** 240–56
Li X-Y and MacBeth C 1997 Data-matrix asymmetry and polarization changes from multi-component surface seismics *Geophysics* **62** 630–43
Liu E R, Yue J H and Pan D M 2006 Frequency-dependent anisotropy: effects of multiple fracture sets on shear-wave polarizations *Chin. J. Geophys.* **49** 1401–9 (in Chinese)
Liu E R *et al* 2003 Observation and analysis of frequency-dependent anisotropy from a multicomponent VSP at Bluebell-Altamont field, Utah *J. Appl. Geophys.* **54** 319–33
Liu K, Zhang Z J, Hu J F and Teng J W 2001 Frequency band-dependence of S-wave splitting in China mainland and its implications *Sci. China* D **44** 659–65
Marson-Pidgeon K and Savage M K 1997 Frequency-dependent anisotropy in Wellington, New Zealand *Geophys. Res. Lett.* **24** 3297–300
Maultzsch S, Chapman M, Liu E and Li X-Y 2003 Modelling frequency-dependent seismic anisotropy in fluid-saturated rock with aligned fractures: implication of fracture size estimation from anisotropic measurements *Geophys. Prospect.* **51** 381–92
Silver P G and Chan W W 1991 Shear wave splitting and subcontinental mantle deformation *J. Geophys. Res.* **96** 16429–54
Thomsen L 1995 Elastic anisotropy due to aligned cracks in porous rock *Geophys. Prospect.* **43** 805–29
Tian X, Zhang J, Si S, Wang J, Chen Y and Zhang Z 2011 SKS splitting measurement with horizontal component misalignment *Geophys. J. Int.* **185** 329–40
Wang Y, Gao Y and Jie M X 2003 The prediction of fractured zone in coal-series strata *J. Chin. Coal Soc.* **28** 566–8
Wei J X 2004 A physical model study of different crack densities *J. Geophys. Eng.* **1** 70–6
Zeng X W and Macbeth C 1993 Algebraic processing techniques for estimating shear-wave splitting in near-offset VSP data: theory *Geophys. Prospect.* **41** 1033–66
Zeng X W and Macbeth C 1998 Vector convolution model and shear-wave splitting algorithm in anisotropic media *Oil. Geophys. Prospect.* **33** 191–97
Zhang J *et al* 2012 The crust and upper mantle anisotropy in Baikal Rift Zone and its dynamic significance *Chin. J. Geophys.* **55** 2523–38 (in Chinese)